

Electronic Supplementary Information

**Near-Unity Electrochemical Conversion of Nitrate to Ammonia on Crystalline Nickel
Porphyrin-Based Covalent Organic Frameworks**

Fang Lv,^{†a,b} Mingzi Sun,^{†c} Yongpan Hu,^{†a,b} Jie Xu,^{a,b} Wei Huang,^{a,b} Na Han,^{*a,b} Bolong Huang^{*c}
and Yanguang Li^{*a,b,d}

^a Institute of Functional Nano & Soft Materials (FUNSOM), Soochow University, Suzhou, 215123
China

^b Jiangsu Key Laboratory for Advanced Negative Carbon Technologies, Soochow University,
Suzhou 215123, China

^c Department of Applied Biology and Chemical Technology, The Hong Kong Polytechnic
University, Hung Hom, Kowloon, Hong Kong SAR, China

^d Macao Institute of Materials Science and Engineering (MIMSE), MUST-SUDA Joint Research
Center for Advanced Functional Materials, Macau University of Science and Technology, Taipa
999078, Macau SAR, China

[†]These three authors contribute equally.

E-mail: yanguang@suda.edu.cn; bhuang@polyu.edu.hk; hanna@suda.edu.cn

Experimental Methods

Preparation of 5, 10, 15, 20-tetrakis (para-aminophenyl)-21H, 23H-porphyrin (H₂Pr): The preparation of H₂Pr was modified from a previous report (*Inorg. Chem.* 1987, **26**, 1009). Typically, 100 mL of nitrobenzene and 12 mL of lactic acid were added to a 250 mL flask and heated at 135°C under magnetic stirring. To this solution was slowly added 12 g of p-nitrobenzaldehyde and 5.3 g of pyrrole dissolved in 70 mL of nitrobenzene via a constant-pressure dropping funnel. The solution was then refluxed at 135°C for 3.5 h. After cooling down to room temperature, the dark purple precipitate was collected by centrifugation, washed with methanol several times, and vacuum-dried at 80°C overnight. To purify the crude product, it was redispersed in 80 mL of pyridine, refluxed at 120°C for 1 h, then cooled to and stored at -4°C overnight. The product was collected by filtration, thoroughly washed with acetone, and vacuum-dried overnight, yielding purple colored 5, 10, 15, 20-tetrakis (p-nitrophenyl) porphyrin (TNP).

For the second step, 3 g of TNP was dissolved in 120 mL of concentrated HCl. It was slowly added with 10 g of SnCl₂·2H₂O dissolved in 50 mL of concentrated HCl at room temperature, and further magnetically stirred for 3 h. The solution was heated to 75°C, reacted at this temperature for 1 h, and then ice cooled for 2 h. The resultant dark green precipitate was collected by centrifugation, redissolved in 300 mL of deionized water, and neutralized with concentrated NH₃·H₂O to pH = 9~10 under stirring. Next, the solid precipitate was collected by centrifugation, washed several times with deionized water, and freeze-dried. It was purified by extraction with 300 mL of chloroform using a Soxhlet extractor. The solvent was finally removed by rotary evaporation to get the titled product as bright purple powders. ¹H NMR (Fig. S20) (400 MHz, DMSO-*d*₆) δ (ppm): 8.89 (s, 8H), 7.85 (d, J = 8.0, 8H), 7.02 (d, J = 8.0, 8H), 5.58 (s, 8H), -2.73 (2H).

Synthesis of 5,10,15,20-tetrakis (4-aminophenyl) porphinato nickel (NiPr): NiPr was synthesized following a previous report (*J. Am. Chem. Soc.* 2020, **142**, 20763). Typically, 100 mg of H₂Pr and 200

mg of Ni(OAc)₂·4H₂O were dissolved in 70 mL of *N,N*-dimethylformamide (DMF) and reacted at 80°C under magnetic stirring and N₂ protection for 24 h. After cooled down to room temperature, the solution was added with deionized water until the precipitation was complete. The resultant purple solid was collected by centrifugation, washed with deionized water three times, and finally vacuum-dried to get the titled product. ¹H NMR (Fig. S21) (400 MHz, DMSO-*d*₆) δ (ppm): 8.77 (s, 8H), 7.65 (d, J = 8.0, 8H), 6.91 (d, J = 8.0, 8H), 5.51 (s, 8H).

Synthesis of NiPr-TPA-COF. 40 mg of NiPr and 20 mg of 1,4-phthalaldehyde were dispersed in a mixed solution of *o*-dichlorobenzene, *n*-butyl alcohol, and 6 M acetic acid (4.4 mL, 5/5/1, v/v/v) in a 15 mL pyrex tube. The tube was then sealed and heated at 120°C for 3 days, yielding a purple precipitate. The solid was then collected via filtration and thoroughly washed with DMF and tetrahydrofuran (THF) several times until the supernatant became colorless. Finally, the product was vacuum dried at 100°C overnight.

Synthesis of H₂Pr-TPA-COF. The synthetic procedure of H₂Pr-TPA-COF was similar to that of NiPr-TPA-COF except for the use of H₂Pr (34 mg, 0.05 mmol) instead of NiPr.

Structural characterizations. Powder XRD was collected on a PANalytical X-ray diffractometer. TEM imaging and EDS mapping were carried out on an FEI Talos F200X transmission electron microscope operating at 200 kV. XPS results were obtained on an Ultra DLD X-ray photoelectron spectrometer. Fourier transform infrared (FT-IR) spectra were collected using a Bruker Vertex 70 FTIR spectrometer in the attenuated total reflection (ATR) mode. Solid-state ¹³C CP-MAS NMR was conducted on a WB 400 MHz Bruker Avance III spectrometer equipped with a standard 4 mm MAS probe head. Liquid ¹H-NMR was performed on a DD2-600 NMR spectrometer. UV-Vis spectroscopy

was performed using a Perkin-Elmer Lambda 750 spectrophotometer. Barret-Emmett-Teller surface areas were measured on a Micromeritics ASAP 2020 HD88 analyzer at 77 K.

Electrochemical measurements. To prepare the working electrode, 1 mg of catalyst power, 0.5 mg of Ketjenblack carbon, and 6 μL of Nafion solution (5 wt%) were dispersed in 250 μL of ethanol and sonicated for 30 min to form a uniform catalyst ink. The catalyst ink was then dropcast onto a $1 \times 1 \text{ cm}^2$ carbon fiber paper and dried at room temperature to achieve an areal loading of 1 mg cm^{-2} . Electrochemical NO_3RR measurements were performed in a custom-designed H-cell. Its two compartments were separated by a Nafion 117 membrane. The H-cell was controlled by a CHI 660E potentiostat, and equipped with a saturated calomel reference electrode (SCE) and a graphite rod counter electrode. The electrolyte was 0.5 M K_2SO_4 containing different concentrations of KNO_3 . It was bubbled by 10 sccm of Ar (99.999%) before and during the reaction to completely remove dissolved O_2 . All the potential readings were recorded against SCE, and compensated for 90% of the ohmic loss. Linear sweep voltammetry (LSV) was collected at a scan rate of 10 mV s^{-1} . Chronoamperometry ($i\sim t$) was carried out at selected working potentials usually for 30 min. The catholyte was then collected and analyzed for dissolved NH_3 using UV-Vis and $^1\text{H-NMR}$.

NH_3 Faradaic efficiency (FE_{NH_3}) was calculated using the following equation:

$$FE_{\text{NH}_3} = \frac{8 \times F \times C_{\text{NH}_3} \times V}{Q_{\text{total}}}$$

where C_{NH_3} was the ammonia concentration in the catholyte, F was the Faraday constant (96485 C mol^{-1}), V was the volume of electrolyte (30 mL), and Q_{total} was the total charge passing the electrode.

NH_3 partial current density (j_{NH_3}) was calculated using the following equation:

$$j_{\text{NH}_3} = j_{\text{total}} \times FE_{\text{NH}_3}$$

NH_3 production rate (r_{NH_3}) was calculated using the following equations:

$$\gamma_{\text{NH}_3} = \frac{C_{\text{NH}_3} \times V}{t \times S}$$

where t was the electrolysis time, and S was the geometric surface area of the electrode (1 cm^2).

Determination of the NH_3 concentration. We used the indophenol blue method for the determination of the NH_3 concentration. First, a series of standard solutions with appropriate NH_4^+ concentrations were prepared by diluting 1000 ppm NH_4^+ standard solution with 0.5 M K_2SO_4 . 2 mL of the above solution was then added with 2 mL of freshly prepared 1 M NaOH solution (containing 5 wt% sodium citrate and 5 wt% salicylic acid), 1 mL of 0.05 M sodium hypochlorite (NaClO) solution and 0.2 mL of 1 wt% sodium nitroferricyanide. It was then incubated in dark at room temperature for 2 h. The UV-Vis absorbance at 655 nm was measured and plotted against the NH_4^+ concentration to construct the calibration curve. Subsequently, catholytes after NO_3RR electrolysis were properly diluted, added with the indophenol indicator, and compared with the calibration curve for the determination of the NH_4^+ concentration. All the measurements were repeated at least three times.

^{15}N isotope labeling experiment. To identify the nitrogen source for NO_3RR , the reaction was carried out at -1.38 V vs. SCE for 2 h in 0.5 M K_2SO_4 + 0.3 M K^{14}NO_3 or 0.5 M K_2SO_4 + 0.3 M K^{15}NO_3 . At the end of the electrolysis, the catholyte pH was adjusted to 2~4 using diluted 0.1 M HCl. 500 μL of the catholyte was added with 100 μL of D_2O solution containing 20 wt% maleic acid as the internal standard, and then analyzed by $^1\text{H-NMR}$ using the water suppression method.

Battery-driven full-cell electrolysis. $\text{IrO}_2@\text{Ti}$ was prepared following a previous report (*Joule* 2019, **3**, 2777). The IrO_2 loading was estimated to be 2 mg cm^{-2} . Coupled $\text{NO}_3\text{RR-OER}$ electrolysis was performed in a single-compartment cell powered by a rechargeable lithium-ion battery. $\text{IrO}_2@\text{Ti}$ (1 cm^2) was used as the OER electrocatalyst; NiPr-TPA-COF loaded on carbon fiber paper was used as the NO_3RR electrocatalyst. The real-time cell voltage between the two electrodes was monitored by a CHI 660 potentiostat connected in parallel; the real-time current density was measured by a 2461-

digital source-meter (Keithley) connected in series. The voltage reading was not compensated for the ohmic loss in this part of the study.

The energy efficiency was calculated using the following equation:

$$\eta = \frac{FE_{NH_3} \times E^0}{E}$$

where E^0 is the theoretical working voltage (1.23 V - 0.69 V = 0.54 V) and E is the actual working voltage of the two-electrode cell.

Computational methods. DFT calculations were applied in this work using the CASTEP packages (*Z. Kristallogr.* 2005, **220**, 567). The generalized gradient approximation (GGA) and Perdew-Burke-Ernzerhof (PBE) functionals (*Phys. Rev. Lett.* 1998, **77**, 3865; *Comput. Phys. Commun.* 2006, **174**, 24; *Phys. Rev. B* 1993, **48**, 4978) were chosen to accurately reveal the exchange-correlation interactions. We selected the ultrasoft pseudopotentials and set the plane-wave basis cutoff energy to 380 eV for all the geometry optimizations. The Broyden-Fletcher-Goldfarb-Shannon (BFGS) algorithm (*Chem. Phys. Lett.* 1985, **122**, 264) was utilized for all the energy minimizations. Considering the computational loading and accuracy, the coarse quality setting of k-points was applied after the convergence tests. In order to achieve the convergence with sufficient accuracy, the following criteria were introduced to evaluate the geometry optimizations: the Hellmann-Feynman forces ≤ 0.001 eV/Å, the total energy difference $\leq 5 \times 10^{-5}$ eV/atom, and inter-ionic displacement ≤ 0.005 Å.

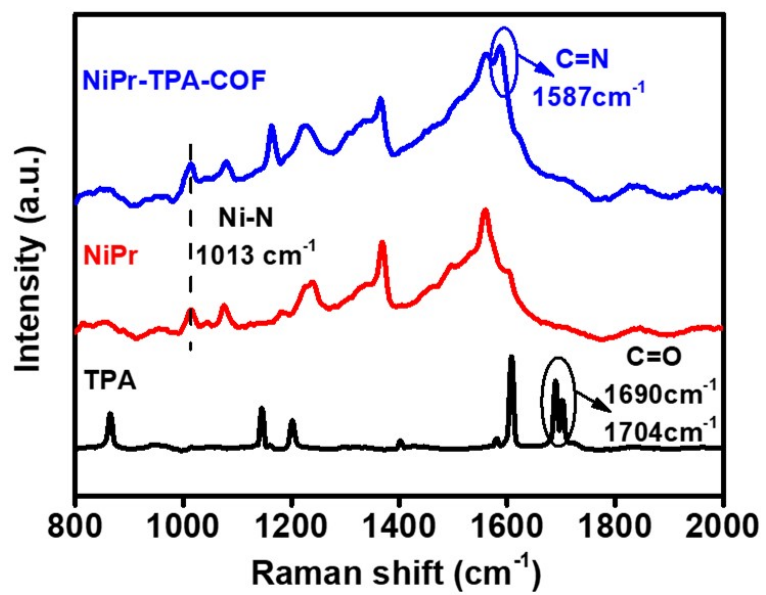


Fig. S1. Raman spectra of NiPr-TPA-COF, NiPr and TPA.

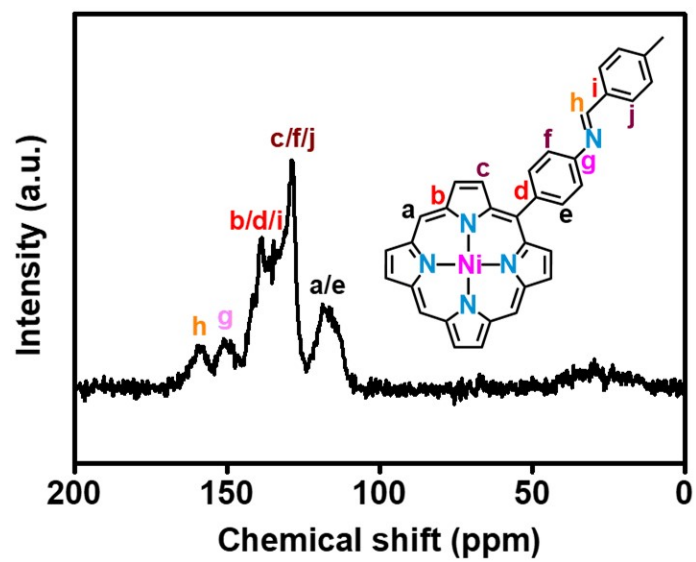


Fig. S2. Solid-state ^{13}C NMR spectrum of NiPr-TPA-COF.

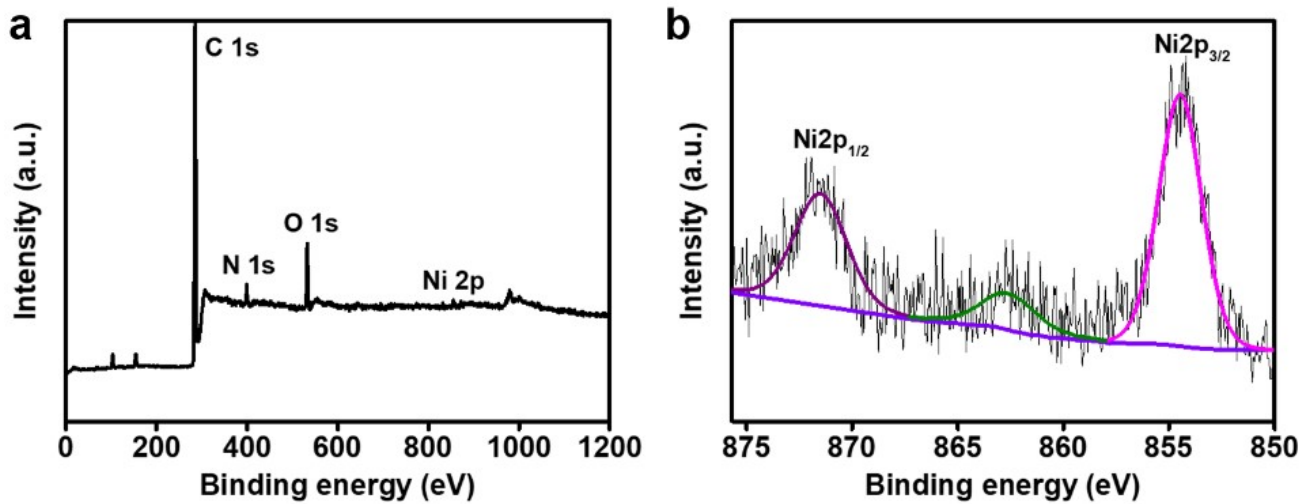


Fig. S3. (a) XPS survey spectrum and (b) Ni 2p XPS spectrum of NiPr-TPA-COF.

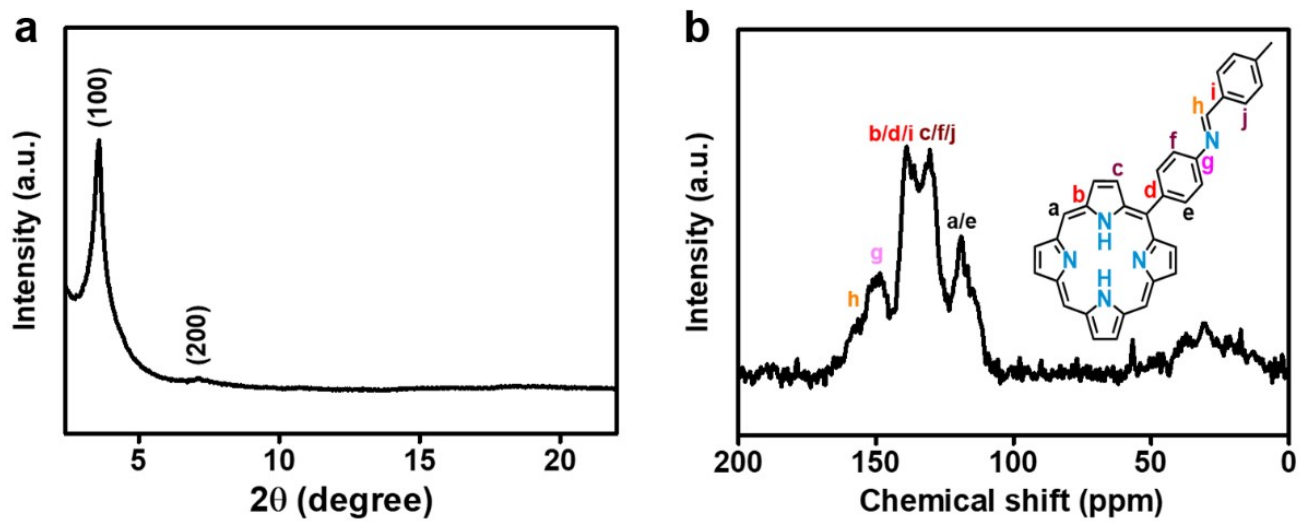


Fig. S4. (a) XRD pattern and (b) solid-state ^{13}C NMR spectrum of H₂Pr-TPA-COF.

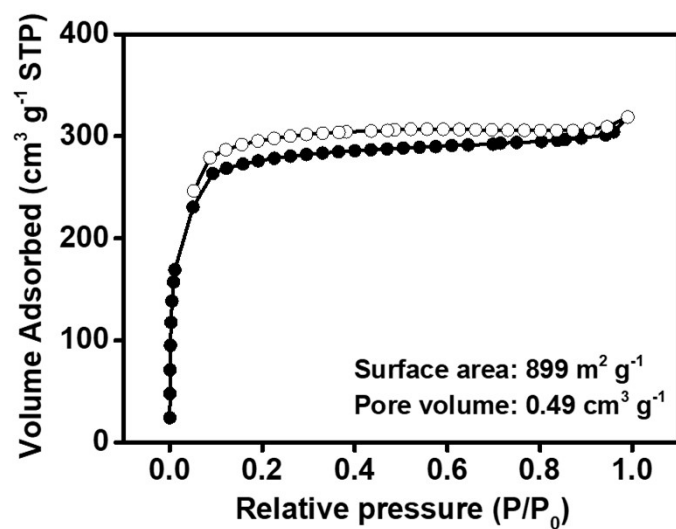


Fig. S5. N₂ adsorption-desorption isotherm of NiPr-TPA-COF.

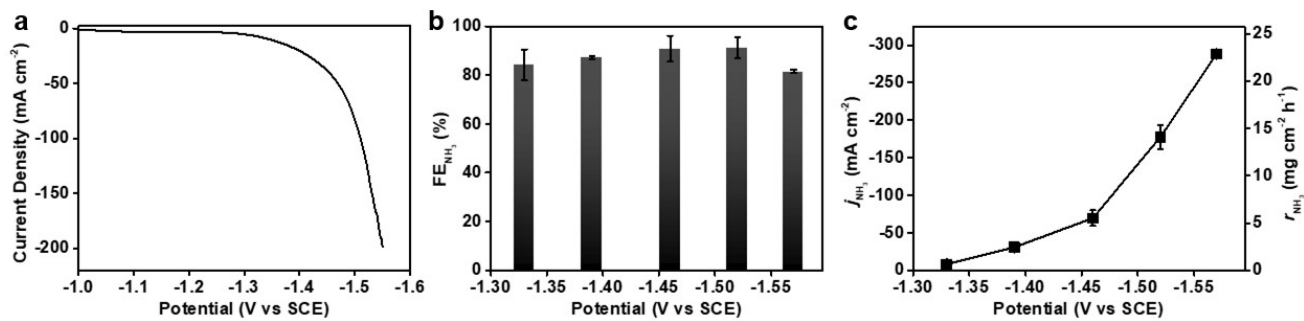


Fig. S6. (a) Polarization curve, (b) NH₃ Faradaic efficiency and (c) NH₃ partial current density and production rate of NiPr-TPA-COF in Ar-saturated 1 M KOH with 0.1 M KNO₃.

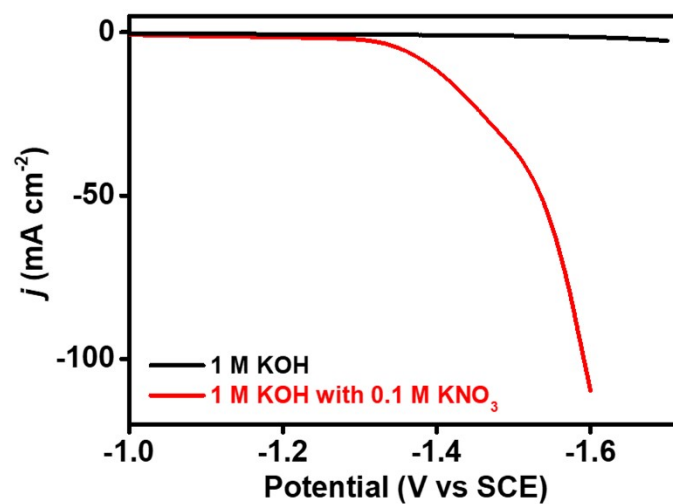


Fig. S7. Polarization curves of the bare carbon fiber paper electrode in Ar-saturated 1 M KOH with and without 0.1 M KNO₃.

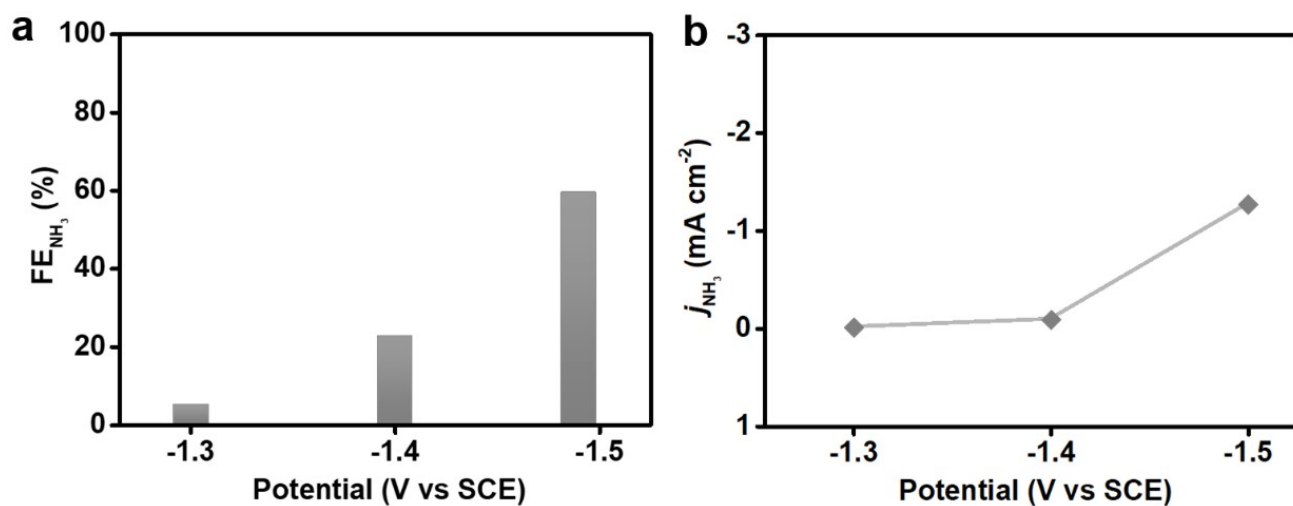


Fig. S8. (a) NH₃ Faradaic efficiency and (b) NH₃ partial current density of the bare carbon fiber paper electrode in Ar-saturated 0.5 M K₂SO₄ with 0.1 M KNO₃.

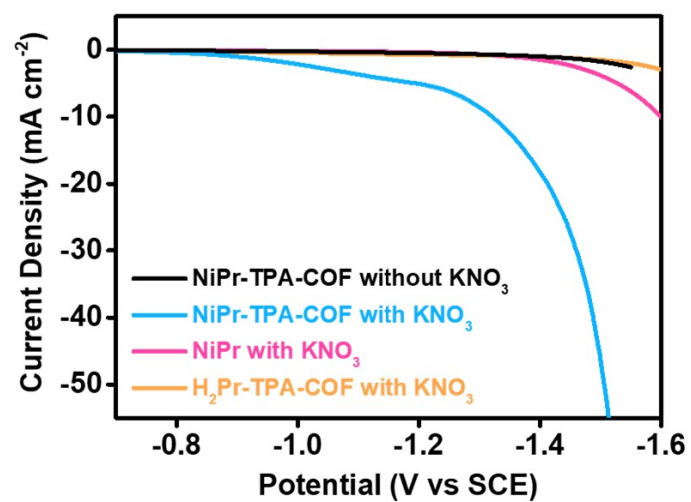


Fig. S9. Polarization curves of NiPr-TPA-COF, H₂Pr-TPA-COF and NiPr in Ar-saturated 0.5 M K₂SO₄ with (or without) 0.1 M KNO₃.

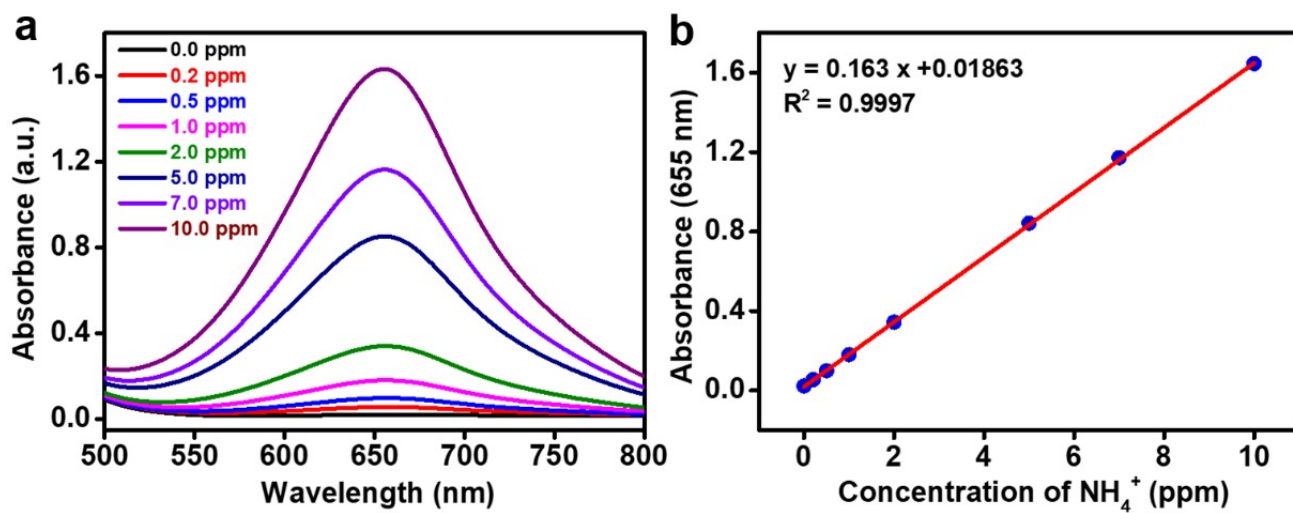


Fig. S10. (a) UV-Vis absorbance of standard NH_4^+ solutions. (b) NH_4^+ calibration curve and corresponding best fitting equation.

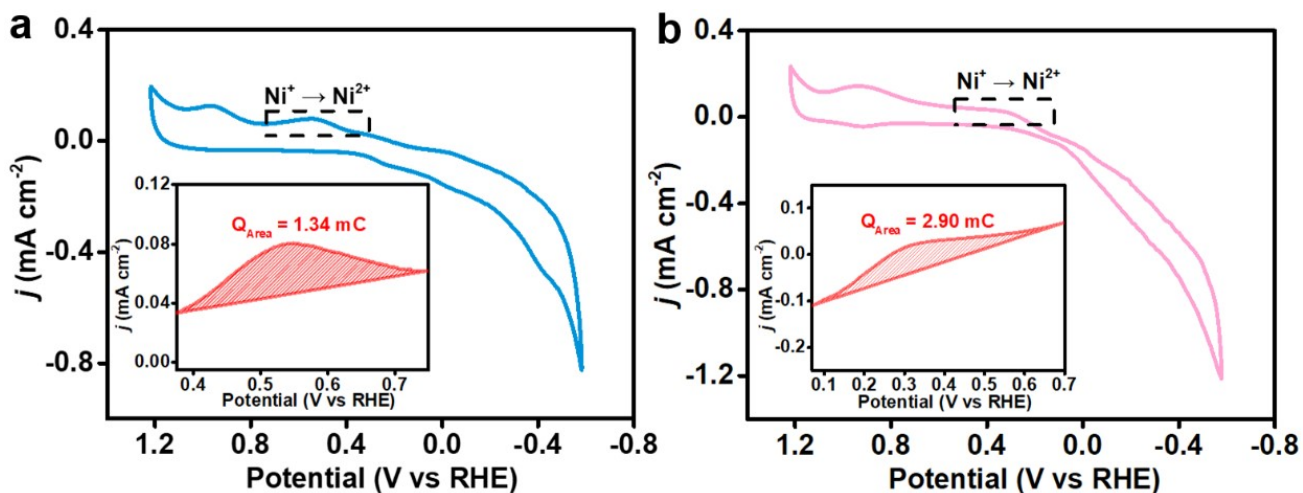


Fig. S11. CV curves of (a) NiPr-TPA-COF and (b) NiPr in Ar-saturated 0.5 M K₂SO₄. Insets show the total charge integrated from the anodic wave of Ni^I/Ni^{II}, which was used to estimate the number of electrochemically active Ni sites as described below.

Turnover frequency (TOF) is defined as the mole of reduction product generated per electrochemically active site per unit time. Taking the calculation of TOF at -1.38 V as an example, the calculation detail is as follows:

First, we calculated the mole of surface active Ni by integrating the anodic wave of Ni^I/Ni^{II} in the CV curve of NiPr-TPA-COF:

$$n_{Ni} = \frac{Q}{F} = \frac{1.34 \text{ mC}}{96485 \text{ C mol}^{-1}} = 1.39 \times 10^{-8} \text{ mol}$$

Then, the TOF was determined as follows:

$$TOF = \frac{j_{NH_3}}{8 \times F \times n_{Ni}} = \frac{15.16 \text{ mA}}{8 \times 96485 \text{ C mol}^{-1} \times 1.39 \times 10^{-8} \text{ mol}} = 1.41 \text{ s}^{-1} = 5076 \text{ h}^{-1}$$

where n_{Ni} was the amount of electrochemically active Ni sites on the working electrode, Q was the integrated charge of the anodic wave, and j_{NH_3} was NH₃ partial current density at -1.38 V vs. SCE.

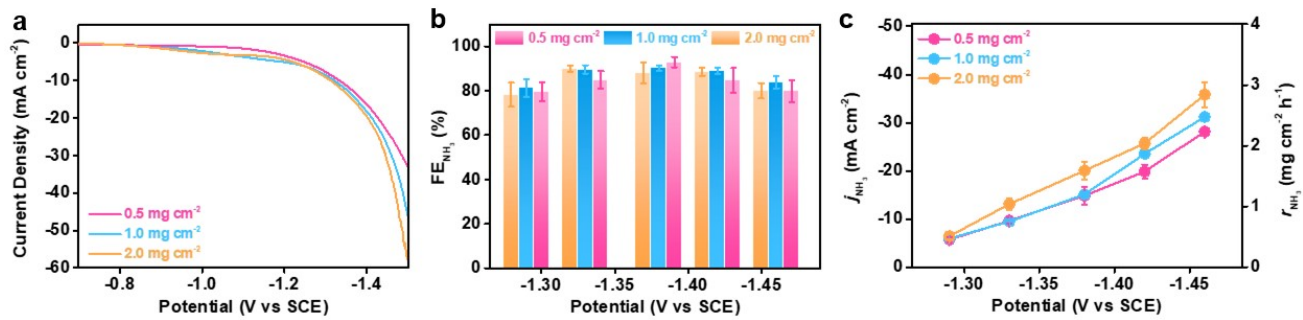


Fig. S12. (a) Polarization curve, (b) NH₃ Faradaic efficiency and (c) NH₃ partial current density and production rate of NiPr-TPA-COF at different catalyst loadings as indicated.

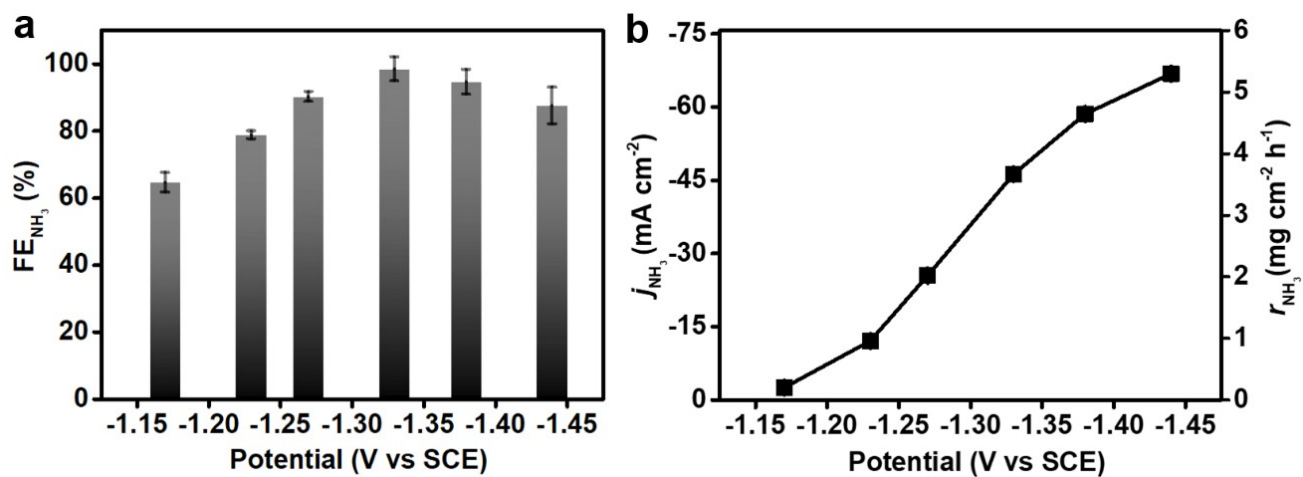


Fig. S13. (a) NH₃ Faradaic efficiency and (b) NH₃ partial current density and production rate of NiPr-TPA-COF in Ar-saturated 0.5 M K₂SO₄ with 0.1 M KNO₂.

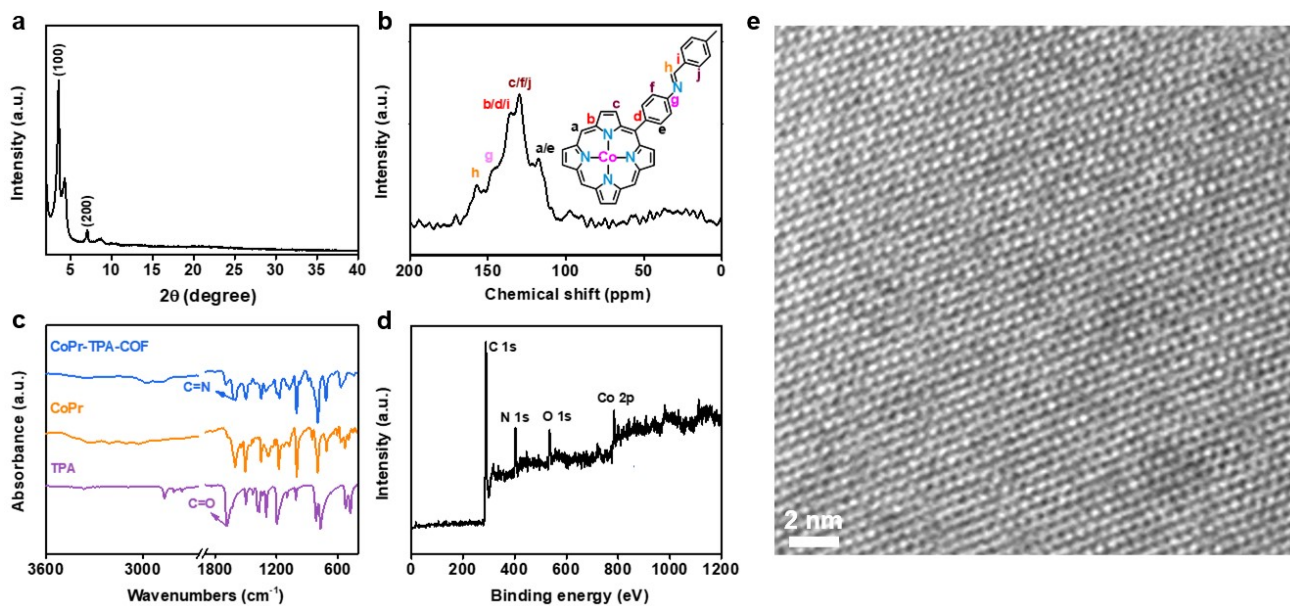


Fig. S14. (a) XRD pattern and (b) solid-state ^{13}C NMR spectrum of CoPr-TPA-COF; (c) FT-IR spectra of CoPr-TPA-COF, CoPr and TPA; (d) XPS survey spectrum and (e) HR-TEM image of CoPr-TPA-COF.

Note that the XRD pattern of CoPr-TPA-COF displays intense diffraction peaks similar to that of NiPr-TPA-COF, indicating highly ordered molecular structure. FTIR and ^{13}C solid-state NMR measurements support the formation of the imine linkage in CoPr-TPA-COF. High-resolution TEM image reveals square lattice fringes. XPS analysis evidences the presence of Co centers.

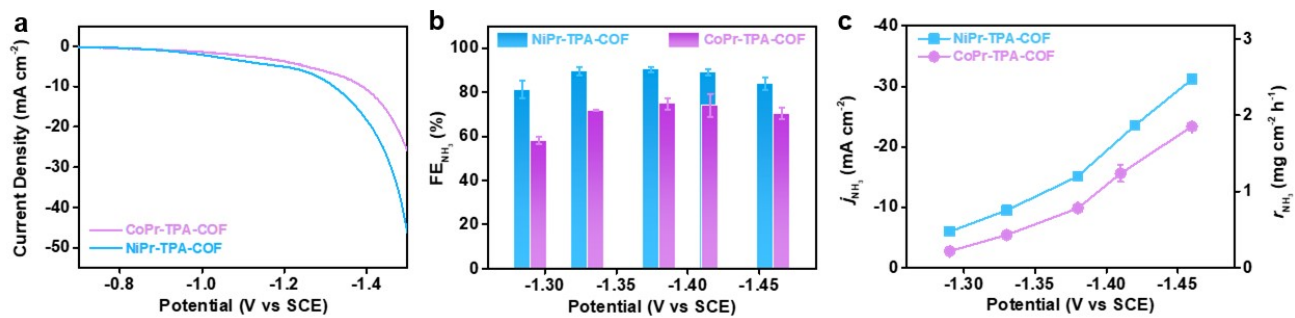


Fig. S15. (a) Polarization curve, (b) NH_3 Faradaic efficiency and (c) NH_3 partial current density and production rate of CoPr-TPA-COF in comparison with those of NiPr-TPA-COF.

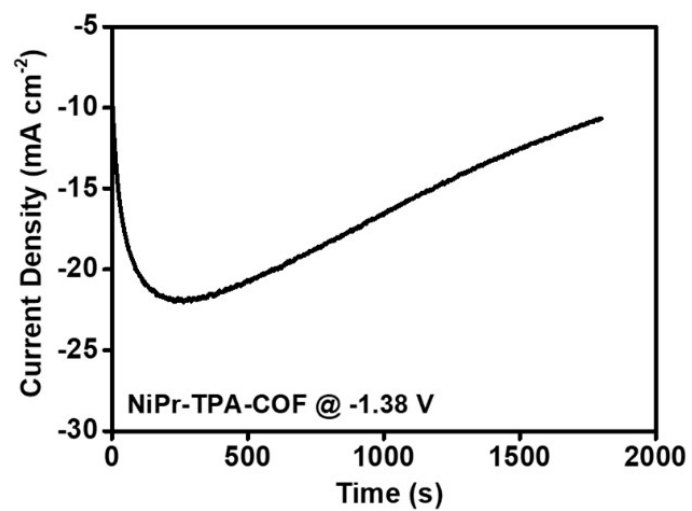


Fig. S16. Chronoamperometric ($i-t$) curve of NiPr-TPA-COF at -1.38 V vs. SCE in 0.5 M K_2SO_4 with 0.1 M KNO_3 .

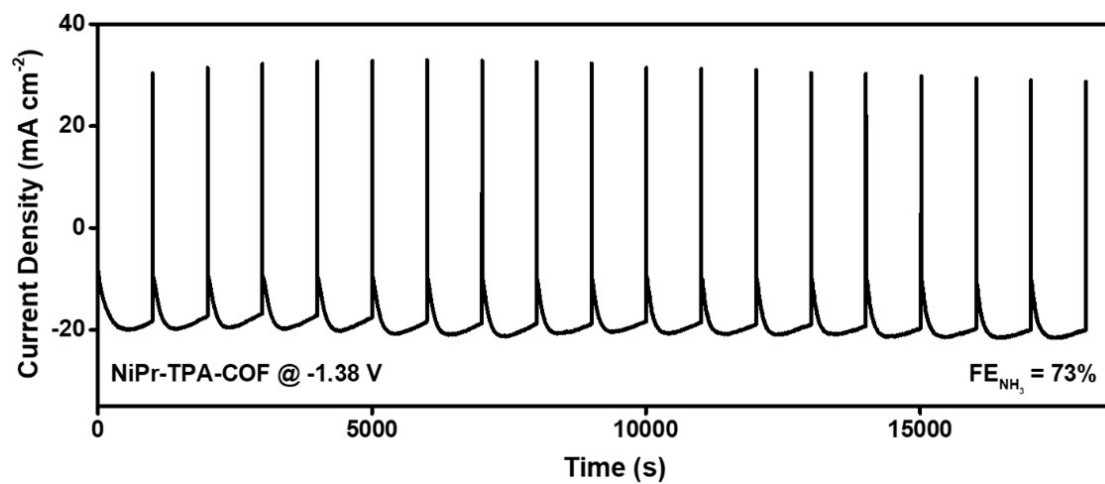


Fig. S17. Pulse electrolysis for NO₃RR on NiPr-TPA-COF. The reduction step was set at -1.38 V for 1000 s, and the oxidation step was set at +0.4 V for 1 s.

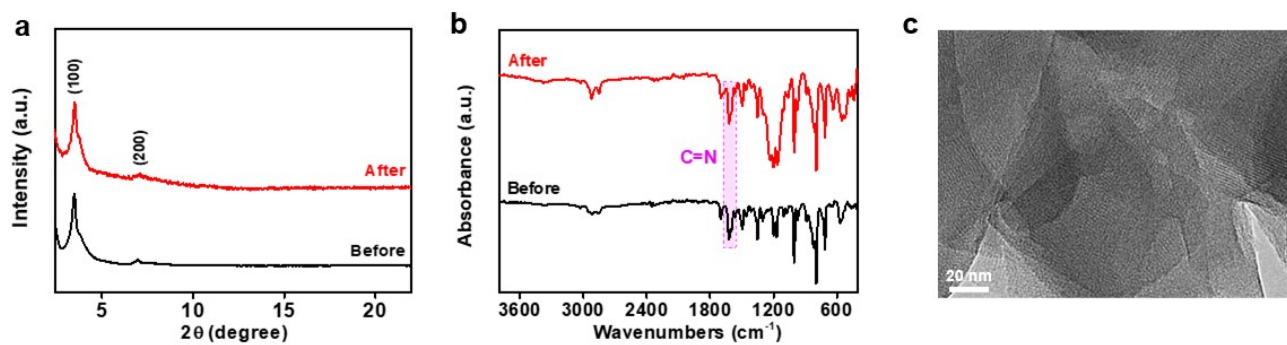


Fig. S18. (a) XRD patterns and (b) FT-IR spectra of NiPr-TPA-COF before and after the long-term electrolysis. (c) TEM image of NiPr-TPA-COF after the long-term electrolysis.

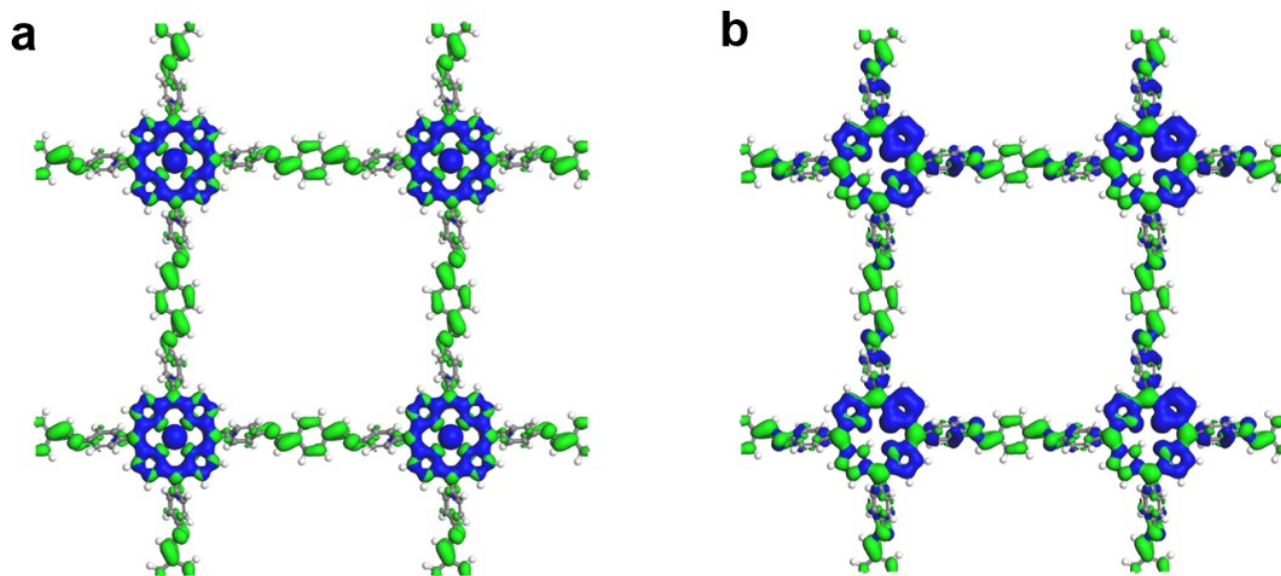


Fig. S19. 3D contour plots of bonding and anti-bonding orbitals near the Fermi level of (a) NiPr-TPA-COF and (b) H₂Pr-TPA-COF.

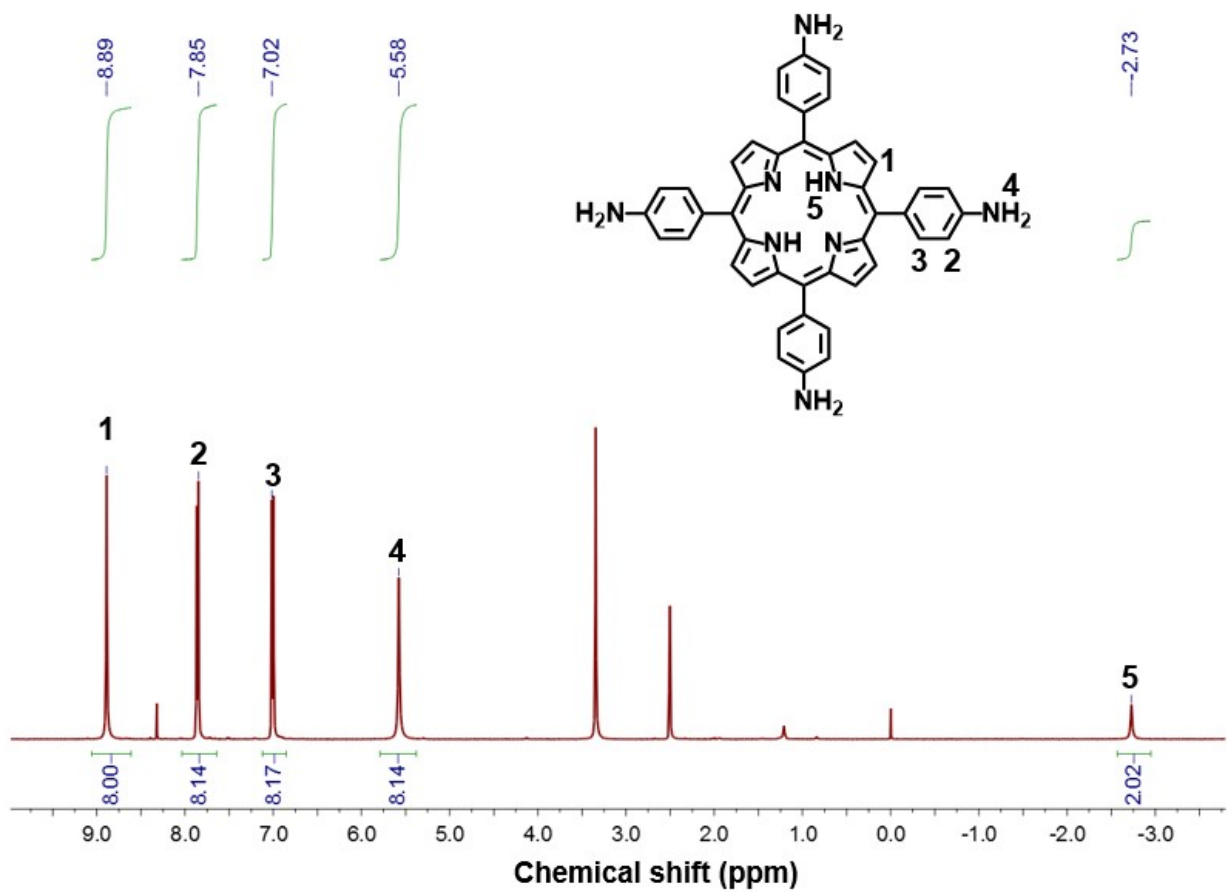


Fig. S20. ¹H-NMR spectrum of H₂Pr.

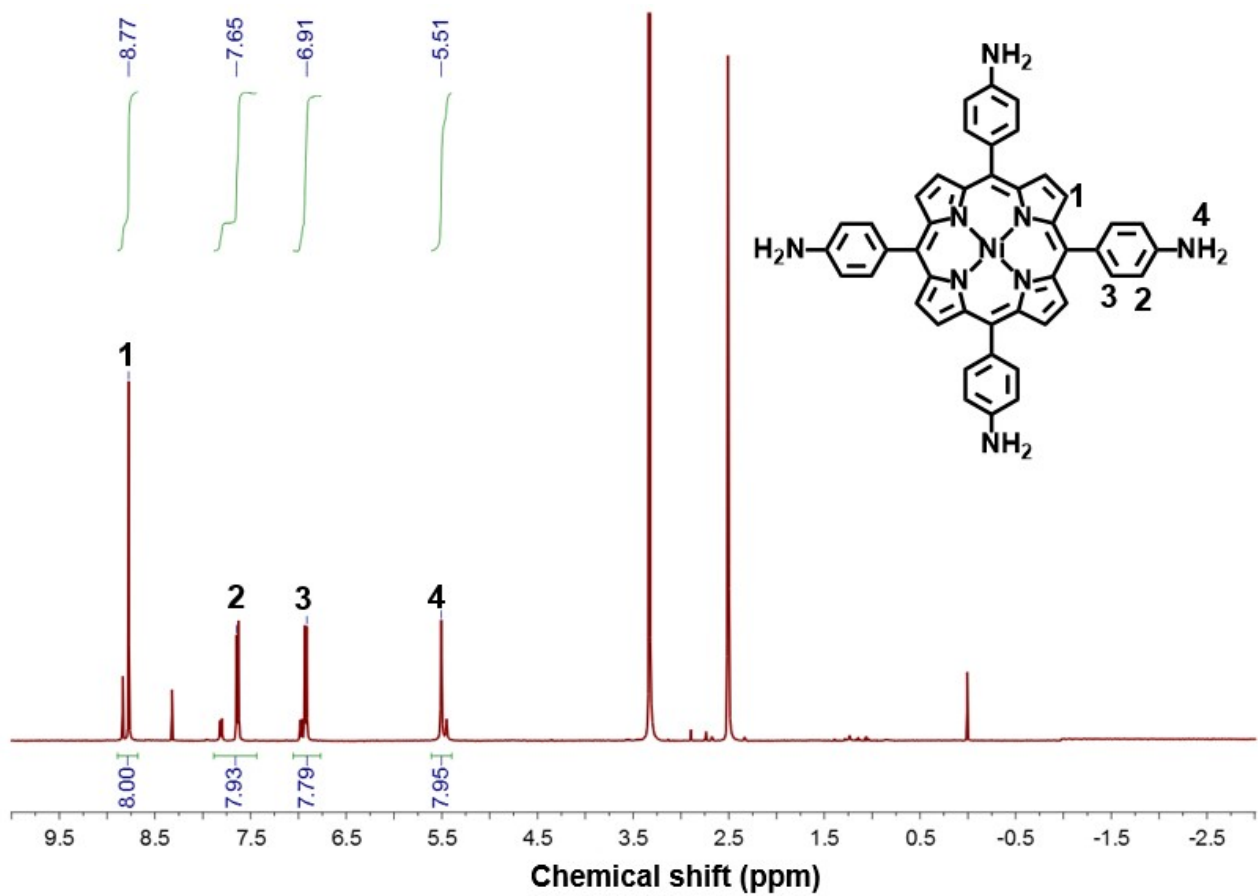


Fig. S21. $^1\text{H-NMR}$ spectrum of NiPr.